Application of the Ellipse of Elasticity Theory to the Functional Analysis of Planar Compliant Mechanisms

O. Sorgonà[a], N. P. Belfiore[b], O.Giannini[a], M. Verotti[c,*]

[a]*Department of Industrial Engineering, Niccoló Cusano University of Rome, Via Don Carlo Gnocchi 18, 00184 Rome, Italy*
[b]*Department of Engineering, Via Vito Volterra, 62, 00146 Roma, Italy*
[c]*Department of Mechanical, Energy, Management and Transportation Engineering, University of Genova Via all'Opera Pia, 15 - 16145 Genoa, Italy*

Abstract

In the last decades, a wide range of methods have been proposed for the analysis of compliant mechanisms. In this investigation, the theory of the ellipse of elasticity is tailored to the linear kinetostatic analysis of flexible systems. The proposed approach exploits the antiprojective polarity transformations of the conic associated to the generic two-port elastic suspension. According to the presented method, the elastostatic features of flexible elements with complex geometries, and of compliant mechanisms with serial, parallel, and hybrid topologies can be represented by a unique geometric entity. As a consequence, the deflection analysis problem is reduced to a geometric problem with a straightforward solution. A specific procedure is developed both at the element and at the mechanism levels, to completely describe field of displacements and loads distribution in the elastic suspension. The application of the method is exemplified considering the analysis of different flexures and of a compliant four-bar linkage.

Keywords: Flexures; Ellipse of elasticity; Parallel compliant mechanisms; Hybrid topologies

Contents

*Corresponding author. *Tel.*:+39 010 3352855
Email address: matteo.verotti@unige.it (M. Verotti)

1. Introduction

In the last decades, compliant mechanisms have been implemented across a variety of applications with a significant growth. In fact, their implementation determines reduction of wear, backlash, lubrication, fabrication time, costs, and compatibility to MEMS-based technologies [1, 2].

Many applications can be found in the areas of precision machining and manufacturing [3, 4], robotics [5, 6], aerospace [7, 8], surgery [9, 10], optics [11, 12], MEMS [13–16], imprint lithography [17, 18] and micropositioning [19–21] systems. In the mechanics field, compliant systems are widely implemented from the design of the single joint [22–25] to the definition of complex mechanisms, such as constant-force [26–28], multi-stable [29, 30], or origami [31, 32] devices.

This increasing trend in terms of applications resulted in a wide range of analytical procedures and design strategies for modeling the deflections of the compliant systems [33]. An initial classification of the various approaches generally considers the deflections amplitude, distinguishing between small and large deflections. In each category, suitable for the resolution of different static problems, many efforts have been done to develop methods of analysis both at the element level and at the mechanism level [34]. Details regarding the methods focused on large deflections, such as elliptic integral solutions [1, 35], pseudo-rigid body models [36, 37], beam and chained beam constraint models [38, 39], can be found in Ref. [40]. In the following, essential notions and recent advances on the methods that fall in the small deflections category are briefly summarized and reviewed.

At the element level, elastic beam theory has been widely implemented to determine analytical formulations describing the characteristics of the deformation. However, the solution of the differential equation of the elastic line may be not trivial for complex geometries, loads and boundary conditions, for example in case of initial curvature and non-uniform cross-sections [41, 42]. Castigliano's theorems have proved to be a useful tools for the analysis of non uniform flexures, such as corner-filleted, elliptic, and hyperbolic flexures [43–45], or other geometries [46–48]. The method leads to the determination of closed-form compliance equations. As for the beam theory, the drawback lies on the determination and solution of the energy equations in case of complex problem. The principle of complementary virtual work has been also applied to the deflections analysis, leading to the complementary virtual work, virtual load, or Maxwell–Mohr methods. In case of linearly elastic materials, the application of this principle is sometimes called method of the virtual work [49]. Belonging to this group, the unit load method [50] was applied to obtain the compliance matrix of flexure hinges [51]. Some efforts have also been made towards the development of generalized [52, 53] or unified [54] compliance models for conic flexures. Finite element analysis was implemented to determine empirical equations for predicting the compliance characteristics of the flexures over large ranges of geometric parameters [55–57]. In other studies, FEA was applied to assess the predictions of the analytical models [58, 59]. However, FEA not always provides an easy identification of the parameters playing a significant role in the deflections, and results depend on the number of elements [60].

Considerable efforts have been made to model small deflections at the mechanism level [61–64]. In this case, the modeling difficulties arise from the kinematic structure of the mechanism. In fact, serial, parallel, and hybrid configurations have been designed to satisfy stiffness, range of motion, mechanical advantage, or amplification ratio requirements [65–69]. The methods described at the element level have been also implemented for the analysis at the mechanism level. For example, beam theory was considered in bridge-type [70–72] and parallel guiding [73, 74] mechanisms. Castigliano's theorem was employed for the analysis of grasping [66, 75], nanopositioning [67, 76], amplification [77, 78], and pointing [79] mechanisms. The analytical formulations obtained with beam theory and Castigliano's theorem have the advantage of giving insight into the deflection problem, but the internal actions analysis can get complicated in complex geometries or configurations [34]. The applicability to a wide range of kinematic chains is the advantage of the finite element method [80, 81] but, as for the element level, its implementation could be time-consuming and results depend on the mesh quality. The compliance matrix method, based on the compliance and stiffness summation of the elements, demonstrated to be a valid tool for the deflection analysis [65, 82–84]. For example, it was applied for modeling parallel [85], XY micropositioning [86, 87], and displacement amplifier

[88] mechanisms. With respect to beam theory and Castigliano's theorem, the compliant matrix method does not require the analysis of the internal actions. However, the output displacement coordinate frame is generally coincident to the input force coordinate frame, condition that is referred to as *single-point* [89]. Furthermore, a detailed displacements analysis requires an additional inverse kinematics step [90] and the modeling procedure becomes complicated in case of multiple actuation forces [34, 91].

Recently, some investigations approached the deflection analysis problem giving more focus on the kinematic aspect, by considering the position of the pole of the displacements. This pole characterizes the rigid displacements consequent to the deflections of the flexible elements [92–94].

In case of linear deflections, it is possible to introduce a fundamental conic section associated to inextensible, shear-rigid, flexible elements. This conic, defined *ellipse of elasticity*, represents an antiprojective polarity transformation between the pole of the displacements and the line of action of the force that causes the deflection. The ellipse of elasticity theory was firstly introduced by Karl Culmann [95] and systematically presented by Wilhelm Ritter, his student and successor [96]. This theory had a significant impact and led to the publication of many studies and handbooks, despite the difficulties related to the extensive usage of projective geometry [97]. More recently, the theory has been recalled in structural analysis investigations [98–100].

In this paper, the ellipse of elasticity theory is applied to the analysis of compliant mechanisms. To the authors knowledge, no prior studies have considered this approach in the compliant mechanisms field. A structured procedure is developed for a comprehensive analysis both at the element level, in case non trivial geometries, and at the mechanism level, in case of parallel, serial or hybrid chains.

The main advantage of the developed approach consists of reducing the deflection analysis problem into a geometric problem, and not into an analytical or numerical one. In fact, deflection analysis can become difficult to solve even for the simplest topologies, whereas the antiprojective polarity properties guarantee a straightforward solution of the geometric problem. Because of the properties of the antiprojective polarity transformation, the ellipse of elasticity represents both the linear compliance function and its inverse, that is the stiffness function. Therefore, both the forward and inverse kinetostatic problems can be geometrically solved, avoiding further geometrical, analytical or numerical steps as, for example, matrix inversions.

More in detail, the key-features of the ellipse of elasticity method are summarized as follows.

- Generality. The theory can be applied to elastic elements with variable curvature and variable flexural rigidity, and to compliant mechanisms with any topology. The elastic problem is always reduced to a geometric problem.
- Kinematic insight. For the specific load condition, the procedure determines the pole of the displacements of the output link with respect to the frame link. Moreover, all the poles of the displacements of the mechanism links,

relative and absolute, can be determined by implementing a back analysis. Therefore, the general displacements field of the mechanism can be determined.

- Load independency. The ellipse of elasticity is not dependent on the load condition. As a consequence, the displacements due to any combined load can be determined by solving a geometric problem, avoiding the re-calculation of the ellipse.
- Multiple-point condition. Because of the previous features, the model overcomes the restriction of the single-point condition. This means that the load-displacement relation can be evaluated for any input and output points, not only in case of coincident points.
- Non-singularity. The load-displacement relation can be evaluated in the particular cases of improper pole of displacements, i.e. pure translations, and of improper line of action, i.e. pure moments.

The remainder of the manuscript is organized as follows. Section 2 introduces the background on projective geometry, that is the base for the application of the theory of the ellipse of elasticity, described in Section 3. Section 4 focuses on the determination of the ellipse parameters for the elastic element, whereas Section 5 describes the implementation of the theory for the analysis of compliant mechanisms characterized by serial, parallel or hybrid kinematic chains. Some examples of the theory implementation are reported at the element level in Section 6, and at the mechanism level in Section 7. Finally, conclusions are presented in Section 8.

2. Projective geometry background

In this Section, the theoretical basis and the fundamental properties underlying the ellipse of elasticty theory are briefly recalled.

2.1. Antiprojective polarity

Every non-degenerate conic section defines a bijective correspondence between the dual sets of points and lines of the projective plane $\mathrm{P}\mathbb{R}^2$, defined as *polarity*. In particular, the polarity defined by imaginary ellipses is equivalent to a bijection associated to real ellipses, defined as *antiprojective polarity*, according to which lines and points become antipolars and antipoles, respectively [101].

With respect to the real ellipse, the properties of the antiprojective polarity transformation can be summarized as follows.

1. External antipolars correspond to internal antipoles.

   With reference to Fig. 1, A_0 and B_0 are two points belonging to the line p. From A_0, it is possible to draw two lines tangent to the ellipse at the points A_1 and A_2. Analogously, B_1 and B_2 are the tangent points of the lines passing through B_0. The line segments $\overline{A_1A_2}$ and $\overline{B_1B_2}$ intersect at

P'. The point P, symmetric of P' with respect to the ellipse center, is the antipole of p.

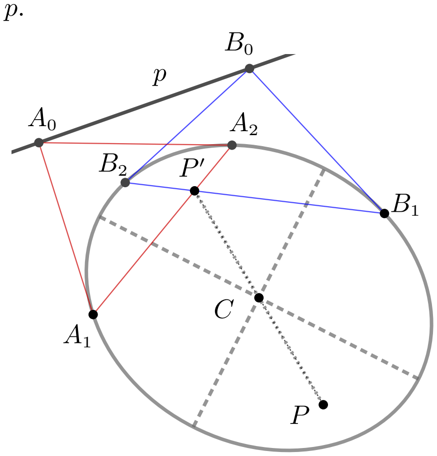

Figure 1: Antiprojective polarity transformation between an external line and an internal antipole.

2. Secant antipolars correspond to external antipoles.

   With reference to Fig. 2, the line p intersects the ellipse at the points A and B. The tangents to the ellipse at A and B intersect at the point P'. The point P, symmetric of P' with respect to the ellipse center, is the antipole of p.

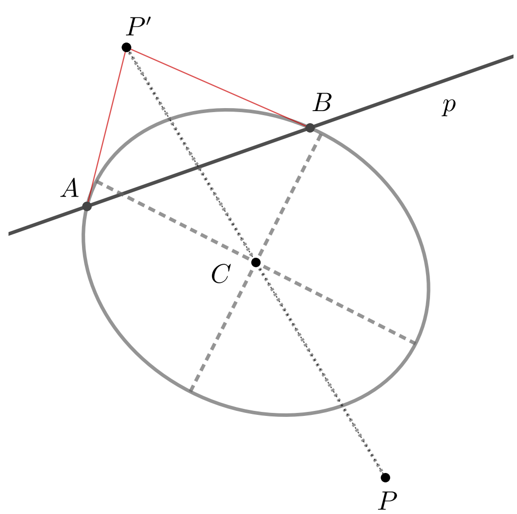

Figure 2: Antiprojective polarity transformation between a secant line and external antipole.

3. Tangent antipolars correspond to antipoles belonging to the conic.

   With reference to Fig. 3, the line p intersects the ellipse at the point P'. The point P, symmetric of P' with respect to the ellipse center, is the antipole of p.

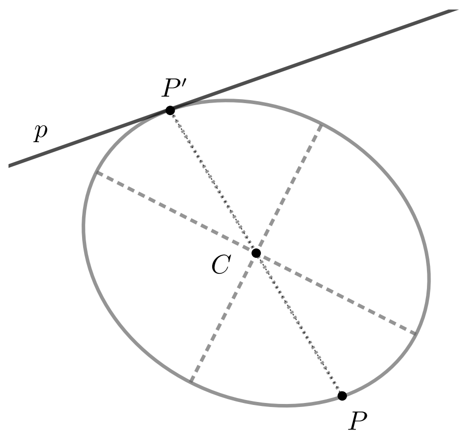

Figure 3: Antiprojective polarity transformation between a tangent line of action and antipole belonging to the ellipse.

4. Antipolar at infinity corresponds to its center; With reference to Fig. 4, the line p is the improper line at infinity. The antipole P coincides with the center of the ellipse C.

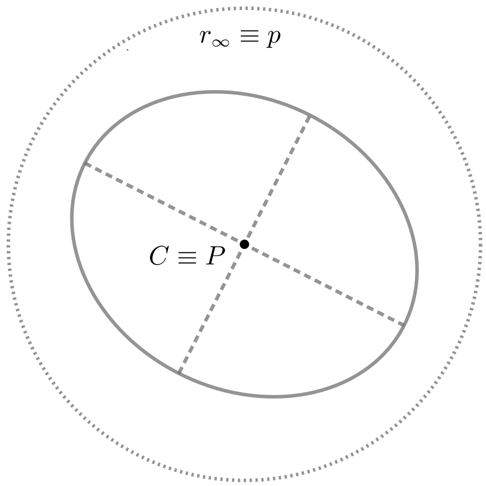

Figure 4: Antiprojective polarity transformation between a line of action at infinity and pole on the center of the ellipse.

5. Antipolars passing through its center correspond to antipoles at infinity.

   Figure 5 shows a particular secant line, passing through the center C. In this case, p is defined as a *diameter* of the ellipse. The tangents t_a and t_b to the ellipse at the points A and B, respectively, intersect at the antipole P at infinity. The line q, parallel to t_a and t_b and passing through C, is also a diameter. In particular, p and q are defined *conjugate diameters* [101]. It is worth noting that, only in the particular case of diameter coincident to an ellipse axis, the tangents are perpendicular to the axis.

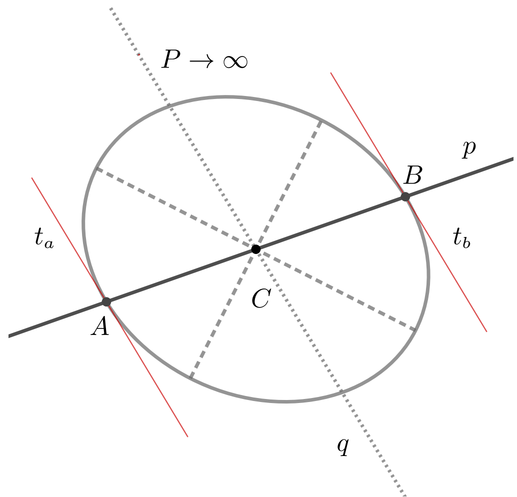

Figure 5: Antiprojective polarity transformation between a line passing through the ellipse center and antipole at infinity.

2.2. Common conjugate diameters

Every two ellipses have one pair of conjugate diameters in common. Without loss of generality, the graphical determination of the pair is based on the assumption that the two ellipses are concentric and intersect to each other in four points [102]. With reference to Fig. 6, the two concentric ellipses intersect in A, B, C, and D. The opposite sides of the parallelogram $ABCD$ are parallel to the common conjugate diameters d' and d'' .

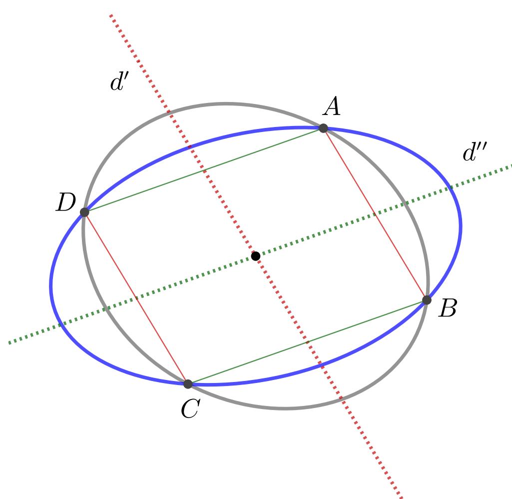

Figure 6: Common chords and conjugate diameters of two ellipses.

3. The ellipse of elasticity theory

The antiprojective polarity transformation, as described in Section 2, can be applied to the analysis of a planar two-port systems composed of two rigid bodies cennected by an elastic suspension. Generally, the suspension can be composed of a single element or of a complex arrangement of flexible and rigid bodies.

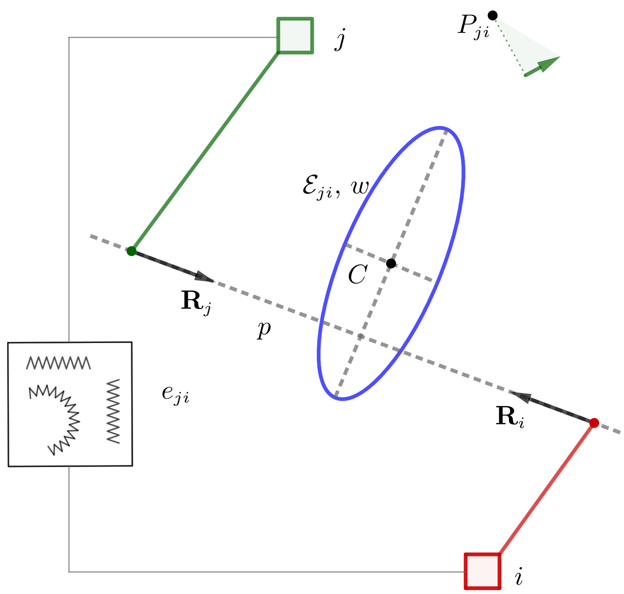

Figure 7: Antiprojective polarity transformation and ellipse of elasticity associated to the elastic suspension e_{ji}.

Figure 7 shows the free-body diagram of a generic two-port system. The loads acting on the bodies can be replaced by a statically equivalent system consisting of the resultants $\mathbf{R}_i$ and $\mathbf{R}_j$, with line of action p. As represented in the figure, resultants are applied to the end sections of the elastic element, directly or by means of a rigid connection.

Since the deflections belongs to the plane, the relative displacement of the rigid bodies can be represented as a rotation with respect to the pole of the displacement P_{ji} [103]. Under the assumption of small deflections, lines of action and poles of the displacement establish an antiprojective polarity transformation, according to the Maxwell's reciprocity theorem [95, 100].

The adoption of a projective geometrical model and the closure at infinity of the affine plane define a comprehensive approach to formulate the planar problem. More specifically, pure moments, associated to the improper line of action, determine displacements whose poles are coincident to the center of the ellipse of elasticity. Analogously, resultants associated to lines of action through the center of the ellipse, determine pure translations, that are displacements whose poles lie at infinity. The translation is parallel to the resultant direction only when the line of action overlaps one of the ellipse axis, as explained in Section 2.

To completely characterize the planar elastic problem, the projective geometrical model must be integrated with information regarding the elastostatic features of the flexible element. This information is conveyed by the *elastic weight* w, a scalar parameter with the physical meaning of a rotational compliance. This parameter can be defined through the relation

$$\theta = w\,M\,, \tag{1}$$

where θ is the relative rotation of the bodies determined by the moment M evaluated at the center of the ellipse. The elastic weight determines also the translational compliances λ_1 and λ_2 along the directions of the ellipse axes, as

$$\lambda_1 = wb^2\,, \tag{2}$$
$$\lambda_2 = wa^2\,, \tag{3}$$

where a and b are the lengths of the semi-axes. Therefore, each ellipse semi-axis length represents the compliance along its perpendicular direction.

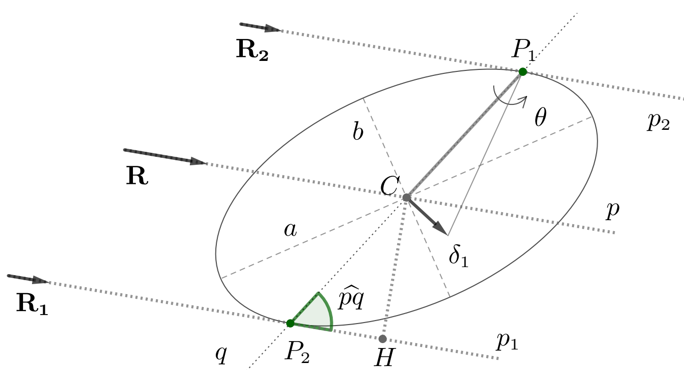

Figure 8: General compliances of translation.

The physical meaning of eqns. (2), (3) can be explained by making use of the antiprojective properties described in Section 2.1. With reference to Fig. 8, resultant $\mathbf{R}$ is decomposed in two forces with equal magnitudes $R_1 = R_2 = R/2$. The lines of action of $\mathbf{R_1}$ and $\mathbf{R_2}$, that are p_1 and p_2, are parallel and tangent to the ellipse in P_2 and P_1, respectively. Points P_1 and P_2 lie on q, that is the conjugate diameter of p. For the antiprojective transformation properties, $\mathbf{R_1}$ determines a rotation θ about P_1. Consequently, the displacement δ_1 of a point initially coincident to C is perpendicular to q and equal to

$$\delta_1 = \theta\,\overline{P_1C}\,. \tag{4}$$

By making use of eqn. (1), eqn. (4) becomes

$$\delta_1 = wR_1\,\overline{HC}\,\overline{P_1C}\,. \tag{5}$$

Since

$$\overline{HC} = \overline{P_2C}\sin\widehat{pq} = \overline{P_1C}\sin\widehat{pq}\,, \tag{6}$$

it follows

$$\delta_1 = wR_1\,\overline{P_1C}^2\sin\widehat{pq}\,. \tag{7}$$

Analogously, $\mathbf{R_2}$ determines a displacement δ_2 equal to

$$\delta_2 = wR_2\,\overline{P_2C}^2\sin\widehat{pq}\,. \tag{8}$$

For the superposition principle, it follows

$$\frac{\delta}{R} = \frac{\delta_1+\delta_2}{R} = w\,\overline{P_1C}^2\sin\widehat{pq} = w\,\overline{P_2C}^2\sin\widehat{pq}\,. \tag{9}$$

If p overlaps the ellipse semi-axis a_1, $\widehat{pq}=\pi/2$ and eqn. (9) becomes

$$\frac{\delta}{R} = \lambda_1 = w\,b^2\,. \tag{10}$$

Analogously, if p overlaps the ellipse semi-axis a_2 it follows

$$\frac{\delta}{R} = \lambda_2 = w\,a^2\,. \tag{11}$$

According to the previous relations, the geometrical model based on the antiprojective polarity transformation becomes a mechanical model able to describe the linear kinetostatic behavior of the two-port elastic suspension.

As stated above, the theory considers the resultant acting on the body. As a consequence, generic combined loads, composed of a force and of a moment, can be reduced to a force with a defined line of action (proper line) or to a pure moment (improper line).

4. Analysis at the element level

Generally, at the element level, the elastic suspension is composed of a beam with variable curvature and variable cross-section. Sections are rigid, plane, and remain plane as the beam undergoes the deformation.

As demonstrated in Refs. [104, 105], the ellipse of elasticity of the beam corresponds to the central ellipse of inertia of its compliance distribution. Therefore, the ellipse of elasticity can be defined by exploiting the geometry of masses theory, from the zeroth-order to the second-order moments, provided that the mass distribution is replaced by the compliance distribution of the element.

Figure 9 shows an initially-curved cantilever beam, with length l, fixed at the origin of the reference frame $\{Oxy\}$. The elastic line is described by means of an arc-length coordinate system with arc-length parameter $s \in [0, l]$.

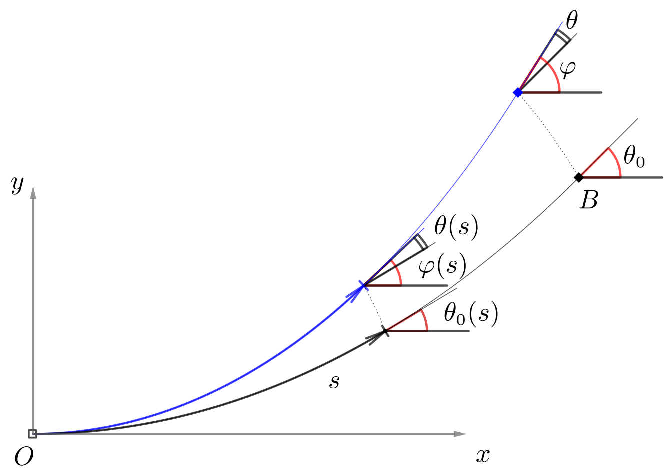

Figure 9: Arc-length coordinate system.

The Euler-Bernoulli beam equation reads

$$\frac{\mathrm{d}\varphi}{\mathrm{d}s} = \frac{1}{r(s)} + c(s)M(s)\,, \tag{12}$$

where $\mathrm{d}\varphi/\mathrm{d}s$ is the rate of change of the section orientation along the beam, $r(s)$ is the radius of curvature in the non-deflected configuration, and $M(s)$ is the internal bending moment. The term $c(s)$, representing the compliance distribution, can be written as

$$c(s) = \frac{1}{\mathrm{E}(s)I(s)}\,, \tag{13}$$

where $E(s)$ is the Young's modulus and $I(s)$ is the moment of inertia of the cross section with respect to the bending axis.

According to Section 1, the elastic weight w can be defined by considering the rotation produced by a pure moment at the free-end section. By separating variables and integrating, eqn. (12) becomes

$$\int_0^{\phi} \mathrm{d}\varphi = \int_0^l \frac{1}{r(s)}\mathrm{d}s + M\int_0^l c(s)\mathrm{d}s\,, \tag{14}$$

or

$$\phi = \theta_0 + \theta\,, \tag{15}$$

where θ_0 is the orientation of the free-end section in the undeformed configuration, and

$$\theta = M\int_0^l c(s)\mathrm{d}s \tag{16}$$

is the rotation of the end-section produced by M. By comparing eqn. (1) and eqn. (16), it follows

$$w = \int_0^l c(s)\mathrm{d}s \;. \tag{17}$$

From a mathematical point of view, the elastic weigth w can be understood as the zeroth-order moment of the function $c(s)$, that is a compliance line distribution. Following this approach, it is possible to exploit the higher-order measures related to the function $c(s)$. In particular, the first-order moments of $c(s)$ with respect to the x- and y-axes are

$$S_x = \int_0^l c(s)y(s)\mathrm{d}s \qquad \text{and} \tag{18}$$

$$S_y = \int_0^l c(s)x(s)\mathrm{d}s\,, \tag{19}$$

respectively. The position of the baricenter C of the distribution can be obtained as

$$x_c = \frac{S_y}{w}\,, \tag{20}$$

$$y_c = \frac{S_x}{w}\,. \tag{21}$$

The point $C \equiv (x_c, y_c)$ is the center of the distribution and the center of the ellipse of elasticity.

Knowing the position of C, it is possible to introduce the central reference frame $\{Cx_0y_0\}$ with origin in C and axis x_0 and y_0 parallel to x and y, respectively. The second-order moments of the compliance distribution with respect to the new frame, that are *central* second-order moments, are given by

$$S_{x_0x_0} = \int_0^l c(s)\, y_0^2(s)\, \mathrm{d}s\,, \tag{22}$$

$$S_{y_0y_0} = \int_0^l c(s)\, x_0^2(s)\, \mathrm{d}s\,, \tag{23}$$

$$S_{x_0y_0} = \int_0^l c(s)\, x_0(s)\, y_0(s)\, \mathrm{d}s\,, \tag{24}$$

and can be arranged in a 2×2 symmetric matrix, as

$$\mathbf{S}_0 = \begin{bmatrix} S_{x_0x_0} & -S_{x_0y_0} \\ -S_{x_0y_0} & S_{y_0y_0} \end{bmatrix}\,. \tag{25}$$

Generally, the second-order moments can be calculated in a reference frame $\{C\xi\eta\}$ that is rotated of the angle α with respect to the frame $\{Cx_0y_0\}$. In particular, if

$$\alpha = \frac{1}{2} \arctan \frac{2S_{x_0 y_0}}{S_{y_0 y_0} - S_{x_0 x_0}} , \tag{26}$$

the central second-order moments become *principal* second-order moments, and their corresponding matrix is

$$\mathbf{S}_{\alpha} = \begin{bmatrix} S_{\xi\xi} & 0 \\ 0 & S_{\eta\eta} \end{bmatrix} , \tag{27}$$

where $S_{\xi\xi}$ and $S_{\eta\eta}$ represent the minimum and maximum values of the moments with respect to α.

Finally, the moments $S_{\xi\xi}$ and $S_{\eta\eta}$ are related to the semi-axes lengths as

$$a_{\xi} = \sqrt{\frac{\mathrm{S}_{\eta\eta}}{w}} , \tag{28}$$

$$a_{\eta} = \sqrt{\frac{\mathrm{S}_{\xi\xi}}{w}} . \tag{29}$$

By comparing eqns.(28) and (29) with (2) and (3), respectively, it follows that $S_{\xi\xi}$ and $S_{\eta\eta}$ represent the principal translational compliances along the axes ξ and η, respectively.

Equations (17), (20), (21), (26), (28) and (29) define elastic weight, center position, semi-axes orientation and semi-axes lengths of the ellipse of elasticity associated to the beam. Therefore, the ellipse results to be completely delineated.

Some examples of determination of the ellipses of elasticity at the element level are reported in Section 6.

5. Analysis at the mechanism level

At the mechanism level, the elastic suspension is composed of sets of rigid bodies connected by means of elastic elements in series, parallel, or hybrid arrangements. In this case, the ellipse of elasticity of the two-port system can be obtained as subsequent composition of ellipses defined by the topology of the arrangement, as explained in the next sub-sections.

5.1. Serial composition of ellipses of elasticity

Figure 10 shows a series arrangement composed of the elastic suspensions e_{ki}, e_{jk}, and of the rigid bodies i, k, and j. The ellipse of elasticity of the series arrangement $\mathcal{E}_{\Sigma}$ can be obtained from the ellipses $\mathcal{E}_{ki}$ and $\mathcal{E}_{jk}$ by exploiting the geometry of masses theory, according to the correspondence described in Section 4 .

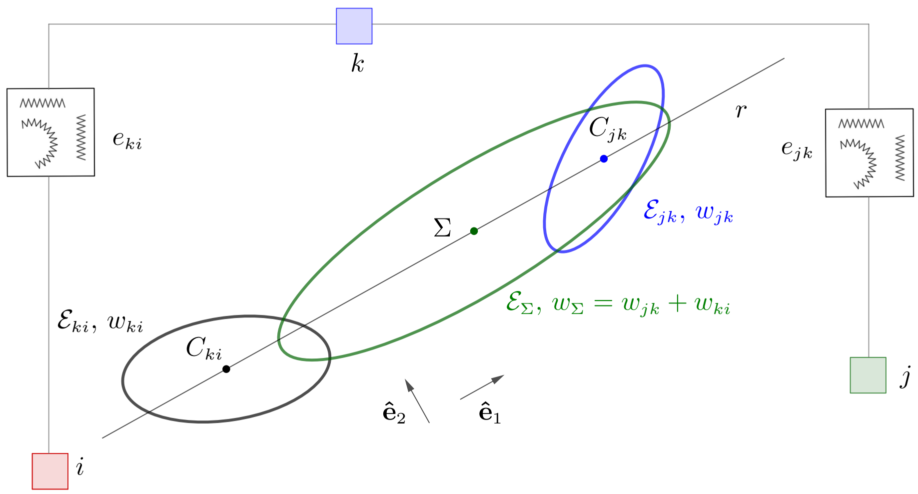

Figure 10: Serial composition of ellipses of elasticity.

Firstly, the resultant elastic weight w_Σ, that is the zeroth-order moment of the total compliance distribution, is given by the sum of the zeroth-order moments of the partial distributions, that corresponds to their elastic weights. Therefore,

$$w_\Sigma = w_{jk} + w_{ki}\ . \tag{30}$$

The center Σ of the total compliance distribution is the center of the ellipse of the series arrangement. According to the definition of *center* of the distribution, the sum of the first-order moments of the elastic weights, with respect to any axis passing through Σ, must be equal to zero, i.e.

$$w_{hi}\overline{C_{ki}\Sigma} = w_{jh}\overline{C_{jh}\Sigma}\,, \tag{31}$$

provided that the elastic weights w_{ki} and w_{jk} are concentrated in the centers C_{ki} and C_{jk} of the ellipses $\mathcal{E}_{ki}$ and $\mathcal{E}_{jk}$, respectively. From eqn. 31, the center Σ, that lies on the line r passing through C_{ki} and C_{jk}, can be found as

$$\frac{\overline{C_{ki}\Sigma}}{\overline{C_{jk}\Sigma}} = \frac{w_{jk}}{w_{ki}}\,. \tag{32}$$

Analogously to the element level, orientation and lengths of the ellipse semi-axes depend on the central second-order moments of the two distributions. In particular, by considering the directions defined by the unit vectors $\hat{\mathbf{e}}_1 \parallel r$ and $\hat{\mathbf{e}}_2 \perp r$, the matrix $\mathbf{S}_{0,\Sigma}$ of the central second-order moments of the serial arrangement reads

$$\mathbf{S}_{0,\Sigma} = \mathbf{S}_{0,ki} + \mathbf{S}_{0,jk} + \begin{bmatrix} 0 & 0 \\ 0 & w_{ki}\overline{C_{ki}\Sigma}^2 + w_{jk}\overline{C_{jk}\Sigma}^2 \end{bmatrix}, \tag{33}$$

where $\mathbf{S}_{0,ki}$ and $\mathbf{S}_{0,jk}$ are the matrices of the central second-order moments of the partial distributions e_{ki} and e_{jk}, respectively. According to the Huygens-Steiner's theorem, the entry $\left(w_{ki}\overline{C_{ki}\Sigma}^2 + w_{hi}\overline{C_{jk}\Sigma}^2\right)$ represents the second-order moments with respect to the perpendicular to r passing through Σ, provided that w_{ki} and w_{jk} are located on the centers C_{ki} and C_{jk}, respectively.

With reference to eqns. (26), (27), matrix $\mathbf{S}_{0,\Sigma}$ can be calculated with respect to the principal reference frame $\{\Sigma\xi\eta\}$, defined by the angle α, as

$$\mathbf{S}_{\alpha,\Sigma} = \begin{bmatrix} S_{\xi\xi} & 0 \\ 0 & S_{\eta\eta} \end{bmatrix}. \tag{34}$$

Finally, the semiaxes lengths can also be calculated by means of eqns. (28), (29), as

$$a_\xi = \sqrt{\frac{S_{\eta\eta}}{w_\Sigma}}, \tag{35}$$

$$a_\eta = \sqrt{\frac{S_{\xi\xi}}{w_\Sigma}}. \tag{36}$$

From the elastic weight w_Σ (Eq. (30)), the position of the ellipse center Σ (Eq. (32)), semi-axes orientation α, and the semi-axes lengths (Eqs. (35) and (36)), the ellipse of the serial arrangement is completely defined. The composition of the ellipses of elasticity is implemented for the analysis of a closed-chain compliant mechanism in Section 7.

5.2. Parallel composition of ellipses of elasticity

Figure 11 shows a parallel arrangement composed of the elastic suspensions e_1, e_2, and of the rigid bodies i and j. The ellipse of elasticity of the parallel arrangement $\mathcal{E}_\Pi$ can be obtained from the ellipses $\mathcal{E}_1$ and $\mathcal{E}_2$ by exploiting the properties of semi-diameters and common conjugate diameters described in Section 2. The unit vectors $\hat{\mathbf{p}}$ and $\hat{\mathbf{q}}$ define the common conjugate diameters (p_1, q_1) and (p_2, q_2) of the ellipses $\mathcal{E}_1$ and $\mathcal{E}_2$, respectively. The unit vectors define also the conjugate semi-diameters (d_{p_1}, d_{q_1}) and (d_{p_2}, d_{q_2}) of $\mathcal{E}_1$ and $\mathcal{E}_2$, respectively.

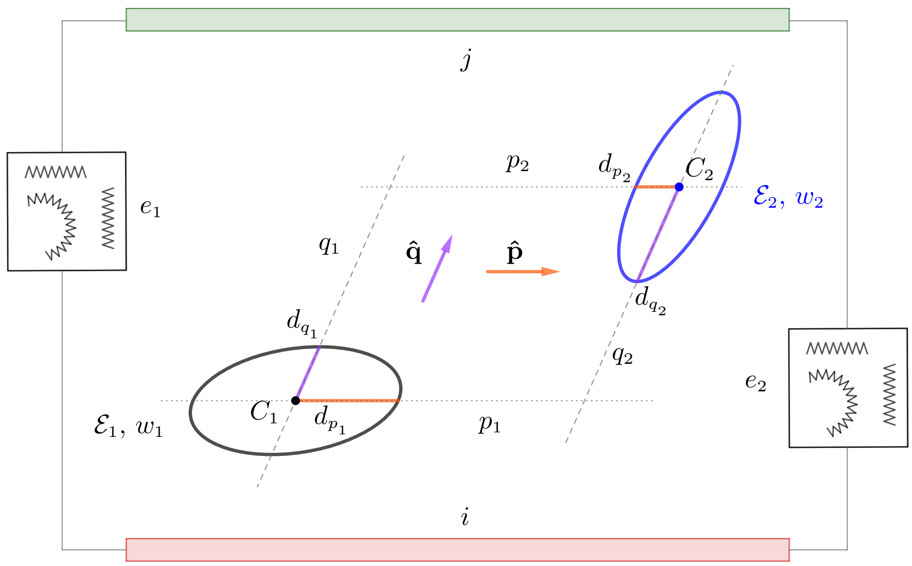

Figure 11: Parallel arrangement

To define the ellipse of the parallel arrangement, two unit translations of the body j with respect to the body i must be considered.

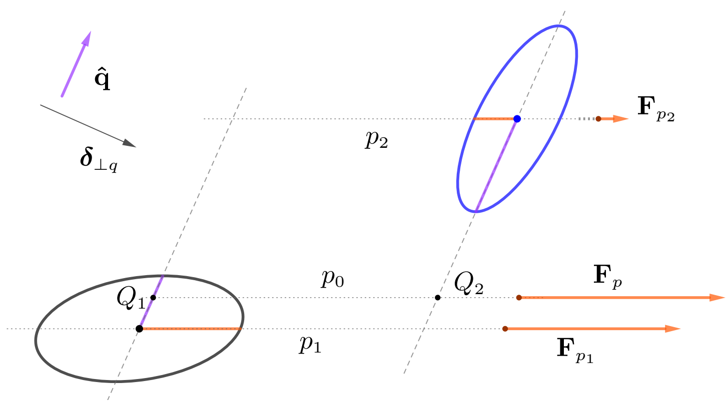

(a) First unit translation.

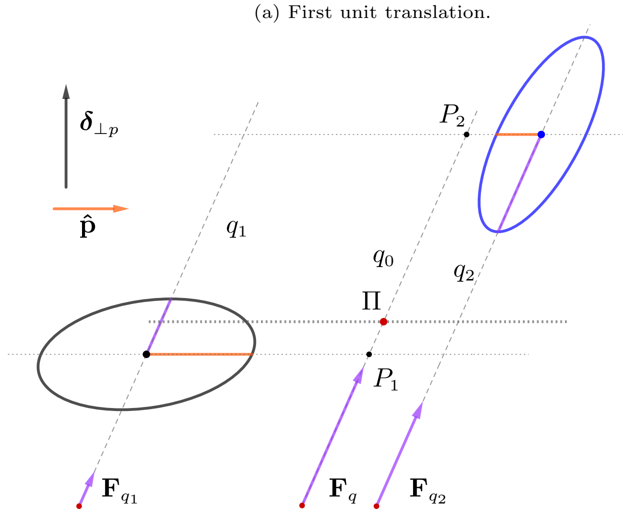

(b) Second unit translation

Figure 12: Unit translations along common conjugate directions to define the center of the parallel ellipse.

With reference to Fig. 12a, the first translation $\boldsymbol{\delta}_{\perp q}$ occurs in the direction perpendicular to q. For the antiprojective properties, $\boldsymbol{\delta}_{\perp q}$ is determined by the system composed of the forces $\mathbf{F}_{p_1}$ on p_1 and $\mathbf{F}_{p_2}$ on p_2. According to eqn. (9) the magnitudes of the forces are

$$F_{p_1} = \frac{1}{w_1 d_{q_1}^2 \sin \widehat{pq}}\,, \tag{37}$$

$$F_{p_2} = \frac{1}{w_2 d_{q_2}^2 \sin \widehat{pq}}\,. \tag{38}$$

The system resultant $\mathbf{F}_p$ is parallel to $\hat{p}$ and its line of action p_0 is given by

$$\frac{\overline{C_1Q_1}}{\overline{C_2Q_2}} = \frac{F_{p2}}{F_{p_1}} , \tag{39}$$

where C_1 and C_2 are the centers of the ellipses $\mathcal{E}_1$ and $\mathcal{E}_2$, respectively, and Q_1 and Q_2 are the intersection points of p_0 with q_1 and q_2, respectively. Equation (39) can be rewritten in terms of the elastic weights and of the geometric parameters of the ellipses by substituting Eq. (37) and Eq. (38) in Eq. (39), obtaining

$$\frac{\overline{C_1Q_1}}{\overline{C_2Q_2}} = \frac{w_1 d^2_{q_1}}{w_2 d^2_{q_2}} . \tag{40}$$

Analogously, with reference to Fig. 12b, the second translation $\boldsymbol{\delta}_{\perp p}$ is determined by the system composed of the forces $\mathbf{F}_{q_1}$ on q_1 and $\mathbf{F}_{q_2}$ on q_2, with magnitudes

$$F_{q_1} = \frac{1}{w_1 d^2_{p_1} \sin \widehat{pq}} , \tag{41}$$

$$F_{q_2} = \frac{1}{w_2 d^2_{p_2} \sin \widehat{pq}} . \tag{42}$$

The system resultant $\mathbf{F}_q$ is parallel to $\hat{q}$ and its line of action q_0 is given by

$$\frac{\overline{C_1P_1}}{\overline{C_2P_2}} = \frac{w_1 d^2_{p_1}}{w_2 d^2_{p_2}} , \tag{43}$$

where P_1 and P_2 are the intersection points of q_0 with p_1 and p_2, respectively.

Lines p_0 and q_0 intersect at point Π, that is the center of the ellipse associated to the parallel arrangement. In fact, p_0 and q_0 are lines of action of forces determining pure translations, as recalled in point (5) of Section 2.

From eqn. (9), it follows

$$\frac{F_p}{\delta_{\perp q}} = \frac{1}{w_1 d^2_{q_1} \sin \widehat{pq}} + \frac{1}{w_2 d^2_{q_2} \sin \widehat{pq}} , \tag{44}$$

$$\frac{F_q}{\delta_{\perp p}} = \frac{1}{w_1 d^2_{p_1} \sin \widehat{pq}} + \frac{1}{w_2 d^2_{p_2} \sin \widehat{pq}} . \tag{45}$$

A translational stiffness matrix $\mathbf{K}$ can be built by considering a reference frame $\{Oxy\}$, where $\hat{\mathbf{e}}_1 \equiv \hat{\mathbf{p}} \parallel p$ and $\hat{\mathbf{e}}_2 \perp p$ are the unit vectors associated to the x- and y-axes, respectively, and O can be any proper point. In this frame, the translational displacement

$$\boldsymbol{\delta} = \begin{Bmatrix} \delta_{\perp q} \sin \widehat{pq} \\ \delta_{\perp p} - \delta_{\perp q} \cos \widehat{pq} \end{Bmatrix} \tag{46}$$

is determined by the force

$$\mathbf{F} = \begin{Bmatrix} F_p + F_q \cos\widehat{pq} \\ F_q \sin\widehat{pq} \end{Bmatrix} . \tag{47}$$

By subtituting Eqs. (44) to (46) in Eq. (47), it follows

$$\mathbf{F} = \mathbf{K}\boldsymbol{\delta} , \tag{48}$$

where

$$\mathbf{K} = \begin{bmatrix} \left(\frac{1}{w_1 d_{p_1}^2} + \frac{1}{w_2 d_{p_2}^2}\right) & \left(\frac{1}{w_1 d_{p_1}^2} + \frac{1}{w_2 d_{p_2}^2}\right)\cot\widehat{pq} \\ \left(\frac{1}{w_1 d_{p_1}^2} + \frac{1}{w_2 d_{p_2}^2}\right)\cot\widehat{pq} & \left(\frac{1}{w_1 d_{p_1}^2} + \frac{1}{w_2 d_{p_2}^2}\right)\cot^2\widehat{pq} \quad + \left(\frac{1}{w_1 d_{q_1}^2} + \frac{1}{w_2 d_{q_2}^2}\right)\frac{1}{\sin^2\widehat{pq}} \end{bmatrix} . \tag{49}$$

With reference to eqns. (26), (27), matrix $\mathbf{K}$ can be calculated with respect to the principal reference frame $\{O\xi\eta\}$, defined by the angle α, as

$$\mathbf{K}_\alpha = \begin{bmatrix} \frac{1}{\lambda_\xi} & 0 \\ 0 & \frac{1}{\lambda_\eta} \end{bmatrix} , \tag{50}$$

where the diagonal entries represent the principal translational stiffnesses.

Regarding the ellipse, the semi-axes lengths can be obtained as

$$a_\xi = \sqrt{\frac{\lambda_\eta}{w_\Pi}} , \tag{51}$$

$$a_\eta = \sqrt{\frac{\lambda_\xi}{w_\Pi}} . \tag{52}$$

The elastic weight w_Π can be calculated by considering a unit rotation about Π of the body j with respect to the body i. According to Eq. (1), the rotation is produced by the pure moment, applied on j,

$$M_0 = \frac{\theta_0}{w_\Pi} = \frac{1}{w_\Pi} . \tag{53}$$

With reference to Fig. 13, M_0 results from the couple of forces $\mathbf{F}_1$, acting on e_1 with line of action r_1, and $\mathbf{F}_2$, acting on e_2 with line of action r_2 parallel to r_1.

Line r_1, that intersects the diameters p_1 in point P_1' and q_1 in Q_1', is the antipolar of Π with respect to the ellipse $\mathcal{E}_1$. Because of the antiprojective polarity properties, it follows

$$\overline{P_1'C_1} \cdot \overline{C_1P_1} = d_{p_1}^2 , \quad \overline{Q_1'C_1} \cdot \overline{C_1Q_1} = d_{q_1}^2 . \tag{54}$$

Analogously, line r_2, that intersects the p_2 in P_2' and q_2 in Q_2', is the antipolar of Π with respect to $\mathcal{E}_2$, and

$$\overline{P_2'C_2} \cdot \overline{C_2P_2} = d_{p_2}^2 \,, \quad \overline{Q_2'C_2} \cdot \overline{C_2Q_2} = d_{q_2}^2 \,. \tag{55}$$

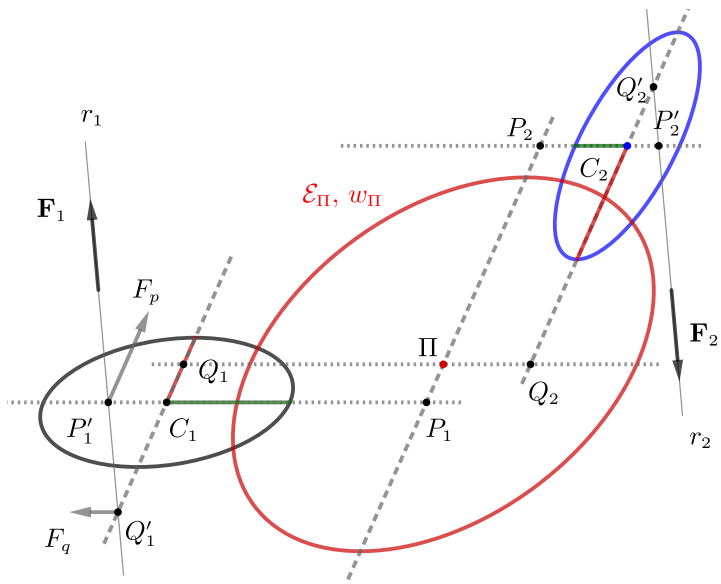

Figure 13: Graphical construction for the determination of the elastic weight of the parallel arrangement.

Because of the parallel arrangement, each force produces the same rotation θ_0. Therefore

$$M_1 = \frac{\theta_0}{w_1} = \frac{1}{w_1} \,, \tag{56}$$

$$M_2 = \frac{\theta_0}{w_2} = \frac{1}{w_2} \,, \tag{57}$$

where M_1 is the moment of $\mathbf{F}_1$ with respect to C_1, and M_2 is the moment of $\mathbf{F}_2$ with respect to C_2.

The moment M_1 can be expressed as

$$M_1 = F_p \sin \widehat{pq}\, \overline{P_1'C_1} \,, \text{ or} \tag{58}$$

$$M_1 = F_q \sin \widehat{pq}\, \overline{Q_1'C_1} \,, \tag{59}$$

where F_p and F_q are the components of $\mathbf{F}_1$ along p and q, respectively. However, the force $\mathbf{F}_1$ can be transformed into the equivalent system composed of $\mathbf{M}_1$ and the force $\mathbf{F}_1'$, whose line of action r_1' is parallel to r_1 and passing through C_1.

With respect to Π, $\mathbf{F}_1'$ produces the moment

$$M_1' = F_p \sin \widehat{pq}\, \overline{C_1P_1} + F_q \sin \widehat{pq}\, \overline{C_1Q_1}\,. \tag{60}$$

By substituting Eqs. (54), (56), (58) and (59) in Eq. (60), it follows

$$M_1' = \frac{1}{w_1}\left(\frac{\overline{C_1P_1}^2}{d_{p_1}^2} + \frac{\overline{C_1Q_1}^2}{d_{q_1}^2}\right). \tag{61}$$

Following an analogous reasoning, the force $\mathbf{F}_2$ can be transformed into $\mathbf{M}_2$ and $\mathbf{F}_2'$, whose line of action r_2' is parallel to r_2 and passing through C_2, producing

$$M_2' = \left(\frac{\overline{C_2P_2}^2}{d_{p_2}^2} + \frac{\overline{C_2Q_2}^2}{d_{q_2}^2}\right). \tag{62}$$

For the equilibrium condition in Π, it follows

$$M_0 = (M_1 + M_1') + (M_2 + M_2'). \tag{63}$$

By substituting Eqs. (53), (56), (57), (61) and (62) in Eq. (63), it follows

$$\frac{1}{w_\Pi} = \frac{1}{w_1}\left(1 + \frac{\overline{C_1P_1}^2}{d_{p_1}^2} + \frac{\overline{C_1Q_1}^2}{d_{q_1}^2}\right) + \frac{1}{w_2}\left(1 + \frac{\overline{C_2P_2}^2}{d_{p_2}^2} + \frac{\overline{C_2Q_2}^2}{d_{q_2}^2}\right). \tag{64}$$

From the elastic weight w_Π (Eq. (64)), the position of the ellipse center Π (Eqs. (39) and (40)), the orientation α, and the semi-axes lengths (Eqs. (51) and (52)), the ellipse of the parallel arrangement is completely defined. As for the series case, the parallel composition of the ellipses of elasticity is implemented in Section 7.

6. Applications at the element level

In this Section, the ellipse of elasticity theory is applied at the element level to the analyses of uniform beams with initial constant curvature and of variable cross-section beams with straight axis.

6.1. Constant-curvature flexure

The elastic element under study is a uniform, constant-curvature beam with radius r, subtending the angle 2θ, with flexural rigidity EI. With reference to Fig. 14, the reference frame Oxy has origin on the arc center and x-axis coincident to the beam axis of symmetry.

6.1.1. Determination of the ellipse of elasticity

According to eqn. (14), the elastic weight of the element is immediately obtained as

$$w = \frac{2r\theta}{EI}\,.$$

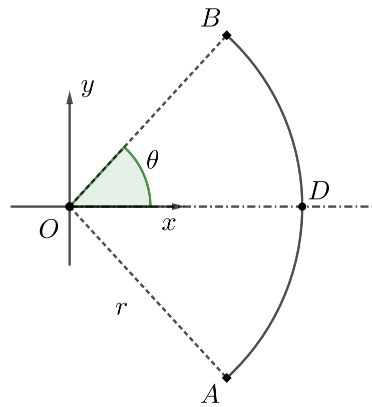

Figure 14: Slender circular beam.

The ellipse of elasticity can be computed by exploiting the symmetry of the element. According to the properties described in Section 4, the center of the ellipse lies on the axis of symmetry, which is also one of the principal directions.

The parametric equations of the arc DB read

$$\begin{array}{l} x = r\cos(\alpha) \\ y = r\sin(\alpha) \end{array} \,, \qquad 0 \leq \alpha \leq \theta \,, \tag{65}$$

hence the abscissa of the center of the ellipse can be determined by making use of eqns. (19),(20), as

$$x_C = \frac{1}{w}\frac{2}{EI}\int_0^{\theta} r^2\cos(\alpha)\mathrm{d}\alpha = r\,\frac{\sin(\theta)}{\theta} \,.$$

The principal second-order moments, according to eqns. (22),(23), read

$$S_{xx} = \frac{2}{EI}\int_0^{\theta} \left[r\sin(\alpha)\right]^2\, r\mathrm{d}\alpha = \frac{r^3}{EI}\left(\theta - \frac{1}{2}\sin(2\theta)\right) \,, \tag{66}$$

$$S_{yy} = \frac{2}{EI}\int_0^{\theta} \left[r\cos(\alpha) - x_C\right]^2\, r\mathrm{d}\alpha = \frac{r^3}{EI}\left(\frac{\cos(2\theta) - 1}{\theta} + \frac{\sin(2\theta)}{2} + \theta\right) \,. \tag{67}$$

Finally, the squared semi-axes of the ellipses can be obtained considering eqns. (28),(29) as

$$a^2 = \frac{r^2}{2}\left(1 - \frac{\sin(2\theta)}{2\theta}\right) \,, \tag{68}$$

$$b^2 = r^2 - (x_C^2 + a^2) \,. \tag{69}$$

It is worth noting that straight beams can be treated as a particular case of constant-curvature beams with curvature tending to zero. For $\theta \to 0$, eqns. (68),(69), become

$$a^2 = l^2 \lim_{\theta \to 0} \left(\frac{2\theta - \sin(2\theta)}{16\theta^3} \right) = \frac{l^2}{12}\,, \tag{70}$$

$$b^2 = l^2 \lim_{\theta \to 0} \left(\frac{\theta^2 - \sin(\theta)^2}{4\theta^4} \right) - \frac{l^2}{12} = 0\,. \tag{71}$$

Therefore, the ellipse of elasticity degenerates in a segment having length $2a$, with $a = l\sqrt{3}/6$.

The ellipses of elasticity of various beams with same unit length and different curvatures are shown in Fig. 15.

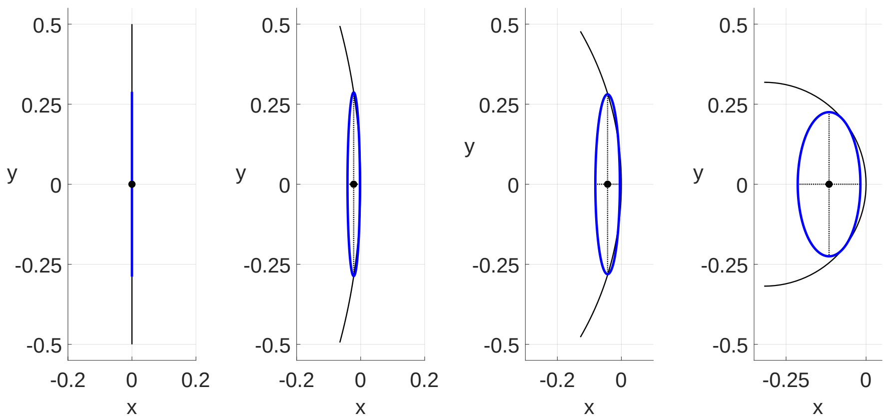

(a) $\kappa = 2\theta/l = 0$; (b) $\kappa = 2\theta/l = \pi/6$; (c) $\kappa = 2\theta/l = \pi/3$; (d) $\kappa = 2\theta/l = \pi$;

Figure 15: Ellipses of elasticity for slender arcs of same lengths and different curvatures.

Straight and initially-curved elements are implemented as element flexures in a planar compliant mechanism in the next sub-section.

6.1.2. *Kinetostatic analysis*

As an example of application at the element level , the beam and its corresponding ellipse of elasticity reported in Fig. 17 are considered.

More specifically, the axis radius is equal to $10/\pi$ mm, and the rectangular cross-section has in-plane dimension equal to 0.1 mm and out-of-plane dimension equal to 0.6 mm. The Young modulus is $E = 2$ GPa. The cantilever is anchored in A and subjected to the resultant force $f = 0.1$ N at the free-end section B, inclined at $-\pi/6$ with respect to the x-axis.

The pole of the displacements of the end-section is determined as the antipole P of the line p with respect to the ellipse $\mathcal{E}$. The moment of the force $\mathbf{f}$ with respect to C produces a rotation

$$\theta = w\,d\,f$$

and a displacement

$$\delta_B = \overline{PB}\theta.$$

The numerical results are reported in Appendix A (case "arc") and compared to the ones obtained by numerical simulations.

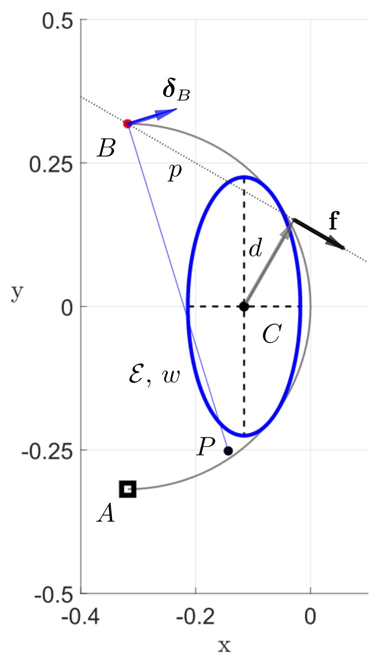

Figure 16: Kinetostatics of a slender arc.

6.2. *Variable cross-section flexure*

Figure 17 shows a variable cross-section flexure and the reference frame Oxy, with origin on the flexure symmetry center and x-axis coincident to the beam axis. For the sake of clarity, a profile that admits a closed-form solution is considered.

Introducing the range

$$x \in [-l/2,\, l/2]\,, \tag{72}$$

where l is the length of the beam axis, the in-plane cross-section profile is defined as

$$h(x) = \frac{\beta l}{\sqrt[3]{1 + \alpha^2(l^2/4 - x^2)}}\,, \tag{73}$$

where α and β are constant. The out-of-plane dimension, t, does not vary along the beam axis.

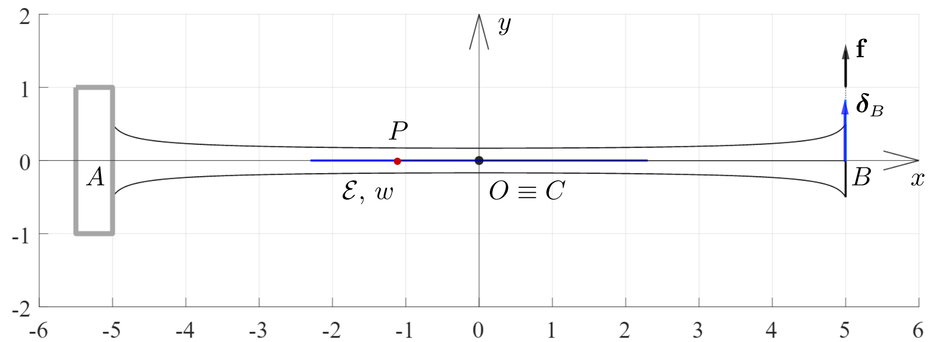

Figure 17: Profile of the variable cross-section flexure, ellipse of elasticity and kinetostatic analysis.

6.2.1. *Determination of the ellipse of elasticity*

According to eqn. (13), the elastic weight of the element is obtained as

$$w = \frac{12}{Et\beta^3 l^2}\left(1 + \frac{l^2}{6}\alpha^2\right) . \tag{74}$$

Because of the symmetry with respect to the x- and y- axes, the center of the ellipse lies on origin O of the reference frame.

The principal second-order moments, according to eqns. (22),(23), are

$$S_{xx} = 0\,, \tag{75}$$

$$S_{yy} = \frac{1}{Et\beta^3}\left(1 + \frac{l^2}{10}\alpha^2\right) . \tag{76}$$

Considering eqns. (28),(29), the squared semi-axes of the ellipses can be obtained as

$$a^2 = \frac{l^2}{20}\frac{(10 + l^2\alpha^2)}{(6 + l^2\alpha^2)}\,, \tag{77}$$

$$b^2 = 0\,. \tag{78}$$

Therefore, as in the case of the uniform straight-axis flexure examined in Section 6.1.1, the ellipse is a degenerate conic section.

6.2.2. *Kinetostatic analysis*

Analogously to the previous case, the flexure with Young modulus equal to $E = 2$ GPa is anchored in A.

The axis length is $l = 10$ mm and the out-of-plane dimension is $t = 0.2$ mm. The in-plane profile was set with $\alpha = 1$ and $\beta = 0.1$. Two different load conditions were considered.

In the first case ("beam (1)" in Appendix A), reported in Fig. 17, a force $f = 0.01$ N along the y direction was applied at the free-end section B. The pole of the displacements is determined as the antipole P of the line p with respect to the ellipse $\mathcal{E}$. The force determines a rotation

$$\theta = w\,\frac{l}{2}\,f$$

and a displacement

$$\delta_B = \overline{PB}\theta.$$

In the second case ("beam (2)" in Appendix A), a moment $M = 0.1$ Nmm was applied at the free-end section. The pole of the displacements is coincident to the center of the ellipse ($O \equiv C$). The moment produces a rotation

$$\theta = w\,M\,f$$

and a displacement

$$\delta_B = \overline{OB}\theta.$$

For both cases, numerical results are reported in Appendix A and compared to the ones obtained by numerical simulations.

7. Application at the mechanisms level

In this Section, the ellipse of elasticity theory is applied at the mechanism level considering a closed-chain compliant mechanism, by implementing the series and the parallel compositions.

7.1. Compliant four-bar

The compliant mechanism under study is the compliant 4-bar linkage shown in Fig. 18. The rigid body 1 represents the fixed frame, whereas external loads are applied to body 4, that serves as input link. As it will be clear in the next subsections, several analyses will be performed focusing on different bodies serving as output link.

7.2. Ellipses at the element level

According to the previous section, the flexible elements are straight and initially-curved beams, with same flexural rigidity, defined by the geometric parameters listed in Table 1. Lengths and coordinates are normalized with respect to a reference length u.

The ellipses of elasticity corresponding to each element are shown in Fig. 19 and defined by the parameters given in Table 2. The elastic weights have been normalized with respect to the the elastic weight w_{12} of the elastic element e_{12}.

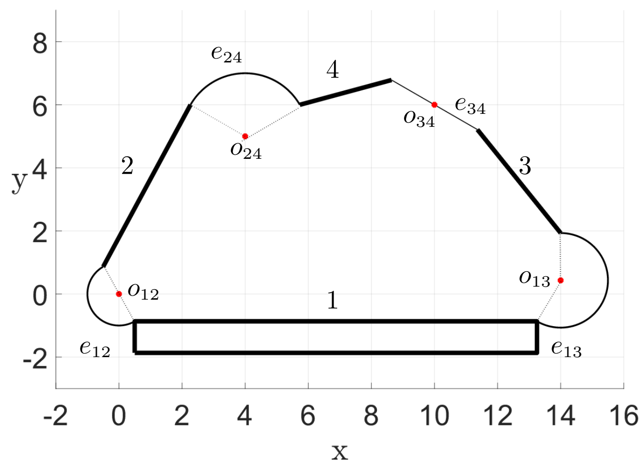

Figure 18: Compliant 4-bar linkage.

Table 1: Geometric parameters of the elastic elements.

Beam	o	r	start angle	amplitude
e_{12}	$(0.00,\ 0.00)$	1.00	$2\pi/3$	π
e_{24}	$(4.00,\ 5.00)$	2.00	$\pi/6$	$2\pi/3$
e_{13}	$(14.0,\ 0.433)$	1.50	$-2\pi/3$	$7\pi/6$
Beam	o	l	orientation	
e_{34}	$(10.0,\ 6.00)$	π	$-\pi/6$	

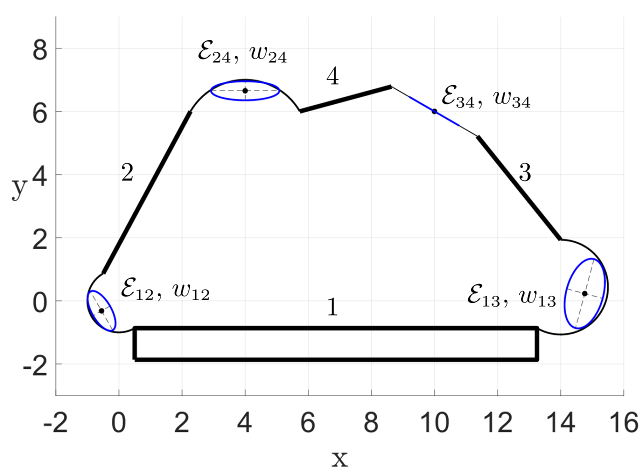

Figure 19: Ellipses of elasticity relative to the elastic elements.

Table 2: Parameters of the ellipses of elasticity: center coordinates, semi-axes lengths, orientations and normalized elastic weights.

Ellipse	Center	a	b	α	w/w_{12}
$\mathcal{E}_{12}$	$(-0.551,\ -0.318)$	0.707	0.308	-1.08	1.00
$\mathcal{E}_{24}$	$(4.00,\ 6.65)$	1.08	0.302	0	1.33
$\mathcal{E}_{13}$	$(14.8,\ 0.228)$	1.13	0.589	1.31	1.75
$\mathcal{E}_{34}$	$(10.0,\ 6.00)$	0.907	0.000	-0.524	1.00

7.3. Compositions of the ellipses of elasticity

The ellipses of elasticity are composed according to the scheme (79). Generally, the composition of the ellipses is not unique, depending on the mechanism topology and on which bodies serve as input and frame links. In this example, body 4 serves as input link, to which the external load is applied. The input link is connected to the frame 1 by means of two chains. The first chain is composed of body 2 and suspensions e_{12} and e_{24}, whereas the second chain is composed of body 3 and suspensions e_{13} and e_{34}. Therefore, the compliant mechanism is analyzed as a parallel composition of two series arrangements.

The first series (1) is composed of the elements e_{12} and e_{24} with associated ellipses $\mathcal{E}_{12}$ and $\mathcal{E}_{24}$, respectively. The second series (2) is composed of the elements e_{13} and e_{34} with associated ellipses $\mathcal{E}_{13}$ and $\mathcal{E}_{34}$, respectively. The ellipses of elasticity of the series, $\mathcal{E}_{\Sigma_1}$ and $\mathcal{E}_{\Sigma_2}$, obtained according to the procedure described in Section 5.1, are shown in Fig. 20.

The two series connect in parallel the frame 1 with the input link 4. The parallel composition of the ellipses $\mathcal{E}_{\Sigma_1}$ and $\mathcal{E}_{\Sigma_2}$ results in the ellipse $\mathcal{E}_{\Pi}$, determined according to the procedure described in Section 5.2. Figure 21 shows the ellipse of elasticity of the parallel arrangement, that is the conic representing the kinetostatic relation between the body 4 and the frame 1.

$$\left.\begin{array}{l}\left.\begin{array}{l}\mathcal{E}_{12}\\ \mathcal{E}_{24}\end{array}\right\} \xrightarrow{\text{Series (1)}} \quad \mathcal{E}_{\Sigma_1}\\[2em] \left.\begin{array}{l}\mathcal{E}_{13}\\ \mathcal{E}_{34}\end{array}\right\} \xrightarrow{\text{Series (2)}} \quad \mathcal{E}_{\Sigma_2}\end{array}\right\} \xrightarrow{\text{Parallel}} \quad \mathcal{E}_{\Pi} \tag{79}$$

Table 3: Parameters of the ellipses of the series and parallel arrangements: center coordinates, semi-axes lengths, orientations and normalized elastic weights.

Ellipse	Center	a_1	a_2	α	w/w_{12}
$\mathcal{E}_{\Sigma_1}$	$(2.05,\ 3.67)$	4.16	0.813	0.980	2.33
$\mathcal{E}_{\Sigma_2}$	$(13.0,\ 2.32)$	3.69	0.805	-0.895	2.75
$\mathcal{E}_{\Pi}$	$(6.61,\ 9.55)$	3.31	2.47	1.49	0.202

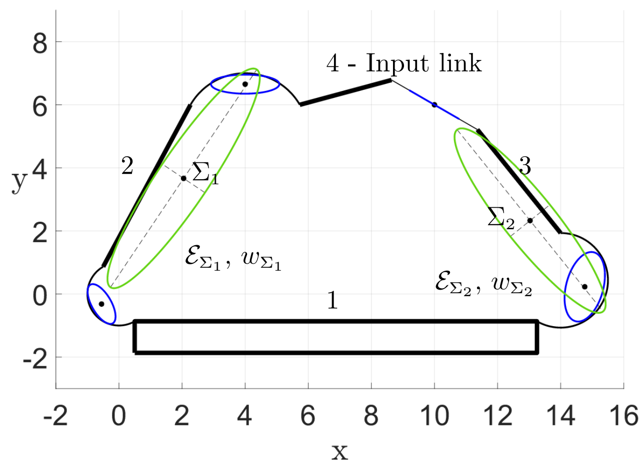

Figure 20: Ellipses of elasticity (green) obtained as series arrangement of two element ellipses (blue).

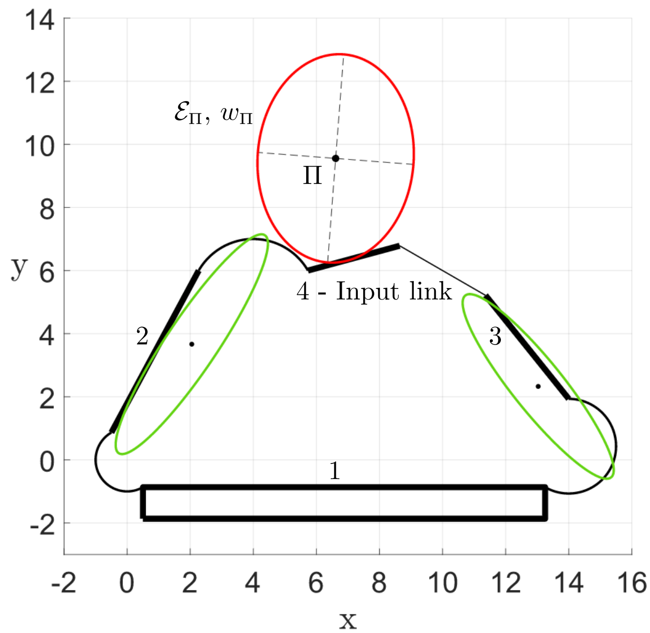

Figure 21: Ellipse of elasticity (red) obtained as parallel arrangement of two ellipses (green).

7.4. Kinetostatic analysis

To perform the kinetostatic analysis, reference length and Young modulus were set as $u = 10$ mm and $E = 70$ GPa, respectively. Out-of-plane dimension was set equal to 5.4 mm, whereas the in-plane flexure width equal to 1 mm. The previous values define the elastic weight $w_{12} = 1$ rad/Nm. A moment $M_0 = 2$

Nm was applied to the input link 4.

The moment produces a rotation

$$\theta_{41} = w_{\Pi} M_0$$

around Π of the body 4. Since the center of rotation and the elastic weight are known, the field of displacements of link 4 is completely defined, as depicted in Fig. 22.

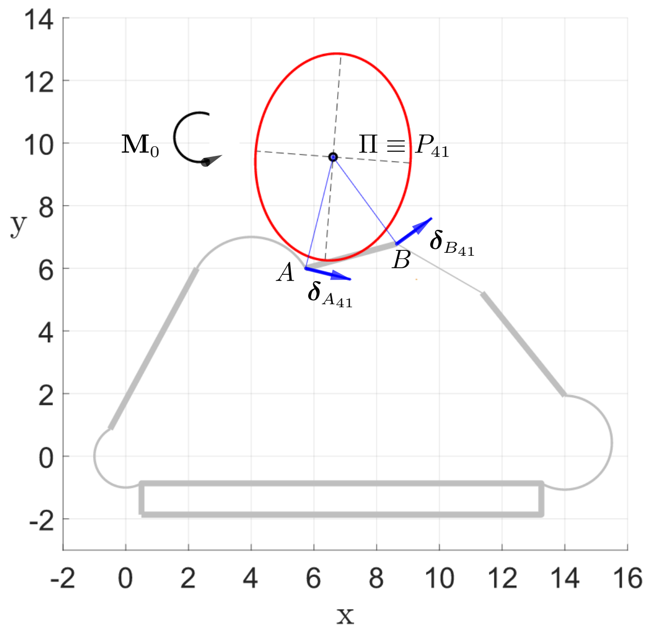

Figure 22: Rotation and displacements of the body 4 due to the application of $\mathbf{M}_0$.

The theory can also be applied to determine the relative and absolute fields of displacements of all the rigid bodies composing the mechanism and the loading distributions on the elastic elements.

For example, with reference to the series arrangement (1), the rotation around Π is produced by a force $\mathbf{f}_1$ whose line of action is the antipolar of Π with respect to the ellipse $\mathcal{E}_{\Sigma_1}$. The force $\mathbf{f}_1$ produces a moment $d_1 f_1 = \theta_{41}/w_{\Sigma_1}$ with respect to the pole Σ_1, as represented in Fig. 23.

The force $\mathbf{f}_1$ affects both the elastic elements e_{12} and e_{24}. Focusing on the displacements of the body 2 with respect to the frame 1, these displacements occur around the center P_{21} that is the antipole of the line of action of $\mathbf{f}_1$ with respect to the ellipse $\mathcal{E}_{12}$, as depicted in Fig. 24. The force $\mathbf{f_1}$ produces a rotation $\theta_{21} = w_{12} f_1 d_{12}$ around P_{21} of the body 2 with respect to the frame 1. Since the center of rotation and the elastic weight are known, the field of displacements of link 2 is completely defined.

In an analogous way, all the relative displacements of the rigid bodies can be

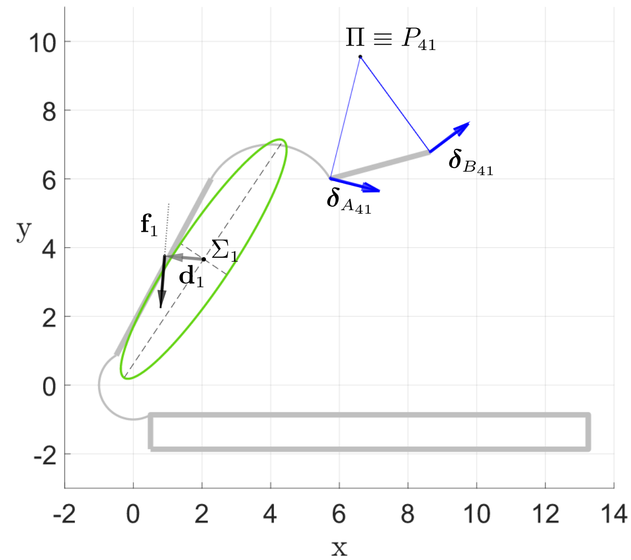

Figure 23: Force acting on the series arrangement (1) consequent to the application of M_0 on the body 4.

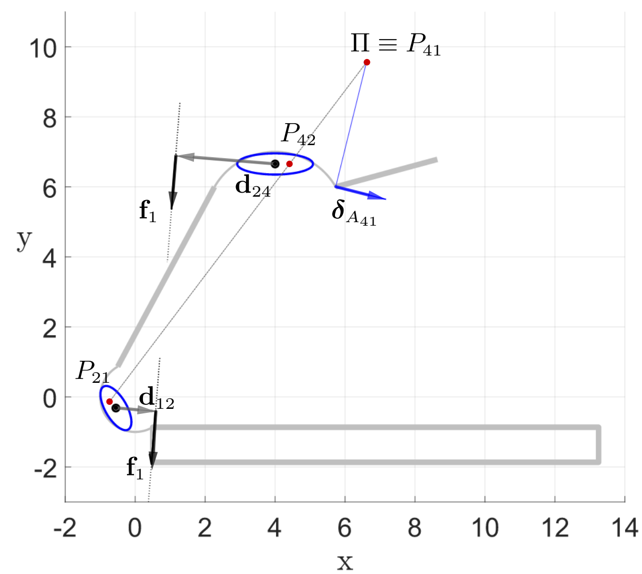

Figure 24: Rotations and displacements of the body 2 and of the body 4 with respect to 2, due to the application of $\mathbf{M}$.

determined, as well as all the corresponding loading conditions. For example, if the ellipse $\mathcal{E}_{24}$ is considered instead of the ellipse $\mathcal{E}_{12}$, the field of displacements of link 4 with respect to the link 2 is completely defined.

With reference to Fig. 24 it is worth noting that, according to the Aronhold-Kennedy theorem, P_{21}, P_{42} and P_{41} lie on the same line.

The numerical values of load magnitudes, rotations, and positions of the poles of displacements are listed in Table 4.

Finally, the procedure followed for the applied moment $\mathbf{M}_0$ can be followed again in the case of the resultant $\mathbf{R}$, and the fields of displacements and loads distributions can be calculated in an analogous way.

Table 4: Load magnitudes, rotations, and positions of the poles of displacement corresponding to each ellipse of elasticity, in the case depicted in Fig. 23 and Fig. 24.

Ellipse	$\mathbf{f}$ (N)	M (Nm)	θ (rad)	$(x_{P_{ij}}, y_{P_{ij}})$ (10^{-2}m)
$\mathcal{E}_{\Pi}$	$(0.000, 0.000)$	2.000	0.405	(6.610, 9.554)
$\mathcal{E}_{\Sigma_1}$	$(-1.195, -15.148)$	0.173	0.405	(6.610, 9.554)
$\mathcal{E}_{12}$	$(-1.195, -15.148)$	-0.173	-0.173	$(-0.735, -0.137)$
$\mathcal{E}_{24}$	$(-1.195, -15.148)$	0.433	0.578	(4.410, 6.652)

8. Conclusions

In this paper, the theory of the ellipse of elasticity has been applied to the linear kinetostatic analysis of compliant mechanisms and a structured procedure has been developed for the analysis both at the element and at the mechanism levels. The method consists of representing the elastic system, regardless its geometric or topological complexity, with a geometric entity not dependent on the load conditions. As a consequence, the deflection analysis problem is transformed into a geometrical problem with straightforward solution. The proposed approach leads to the complete description of the fields of displacements and of the loads distribution in the compliant system, for any applied load.

The method proven to be effective in case of uniform elements, with straight axis and with constant-curvature axis, and in case of variable cross-section elements. A the mechanism level, the method was implemented for the analysis of a closed-chain four-bar compliant linkage. Finite element analyses confirm the validity of the results.

Appendix A. Numerical analysis

To validate the proposed theory, finite element simulations were performed with the commercial software Ansys.

At the element level, the constant-curvature cantilever flexure and the variable cross-section element, analyzed in Section 6.1.2 and in Section 6.2.2, respectively, were considered for the numerical analyses. The generated mesh of the variable cross-section element is shown in Fig. A.25.

At the mechanism level, Fig. A.26 shows the mesh of the compliant four-bar linkage, particularly refined in the flexible regions.

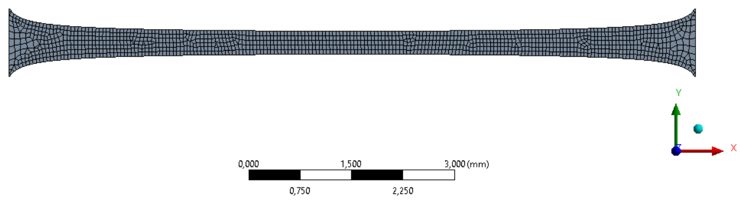

Figure A.25: Variable cross-section beam: generated mesh.

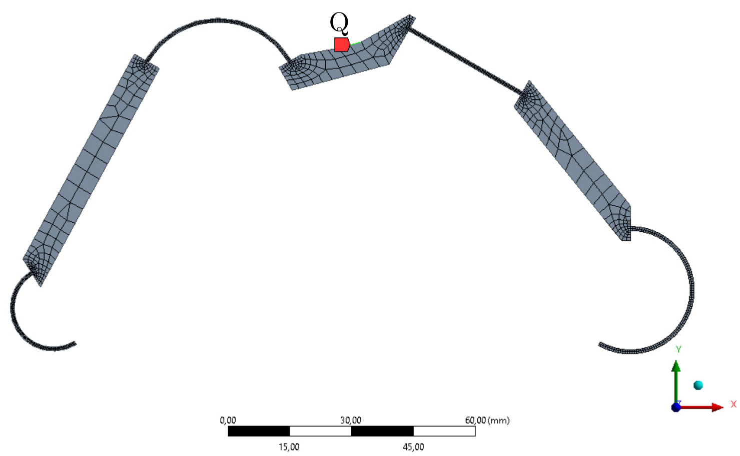

Figure A.26: Compliant four-bar linkage: mesh and output point Q.

For all the cases, Young modulus, load and constraint conditions are the same of the theoretical approach.

The results of the simulations at the element and at the mechanism levels are reported in Tables A.5 and A.6, respectively, and compared to the theoretical ones. For each case, the table lists rotation and mid-point displacement of the output end-section or link, in case of element or mechanism system, respectively.

Table A.5: Theoretical and FEA results comparison at the element level.

Flexure	theory			FEA			err. (%)		
	δ_x (mm)	δ_y (mm)	θ (rad)	δ_x (mm)	δ_y (mm)	θ (rad)	δ_x	δ_y	θ
arc	0.994	0.305	-0.174	0.987	0.304	-0.172	0.71	0.33	1.16
beam (1)	0	1.600	0.265	0	1.616	0.268	-	0.99	1.12
beam (2)	0	2.650	0.530	0	2.672	0.544	-	0.82	2.57

Table A.6: Theoretical and FEA results comparison at the mechanism level.

Four-bar	theory			FEA			err. (%)		
	δ_x (mm)	δ_y (mm)	θ (rad)	δ_x (mm)	δ_y (mm)	θ (rad)	δ_x	δ_y	θ
Point Q	12.789	2.329	0.405	12.360	2.248	0.393	3.47	3.60	3.05

Results show a very good agreement between theoretical and numerical approaches, with error less than 1% and about 3% at the element and mechanism level, respectively.

References

[1] L. Howell, Compliant Mechanisms, Wiley, New York, 2001.

[2] M. Verotti, A. Dochshanov, N. P. Belfiore, A comprehensive survey on microgrippers design: Mechanical structure, Journal of Mechanical Design 139(6) (2017) 060801.

[3] Y. Tian, B. Shirinzadeh, D. Zhang, A flexure-based mechanism and control methodology for ultra-precision turning operation, Precision Engineering 323(2) (2009) 160–166.

[4] Y. Tian, D. Zhang, B. Shirinzadeh, Dynamic modelling of a flexure-based mechanism for ultra-precision grinding operation, Precision Engineering 35(4) (2011) 554–565.

[5] P. Bilancia, M. Baggetta, G. Berselli, L. Bruzzone, P. Fanghella, Design of a bio-inspired contact-aided compliant wrist, Robotics and Computer-Integrated Manufacturing 67 (2021) 102028.

[6] T. Morales Bieze, A. Kruszewski, B. Carrez, C. Duriez, Design, implementation, and control of a deformable manipulator robot based on a compliant spine, The International Journal of Robotics Research 39(14) (2020) 1604–1619.

[7] E. G. Merriam, J. E. Jones, S. P. Magleby, L. L. Howell, Monolithic 2 DOF fully compliant space pointing mechanism, Mechanical Sciences 4(2) (2013) 381–390.

[8] W. Zeng, F. Gao, H. Jiang, C. Huang, J. Liu, H. Li, Design and analysis of a compliant variable-diameter mechanism used in variable-diameter wheels for lunar rover, Mechanism and Machine Theory 125 (2018) 240–258.

[9] S. Kota, K.-J. Lu, Z. Kreiner, B. Trease, J. Arenas, J. Geiger, Design and application of compliant mechanisms for surgical tools, Journal of Biomechanical Engineering 127(6) (2005) 981–989.

[10] T. L. Thomas, V. Kalpathy Venkiteswaran, G. Ananthasuresh, S. Misra, Surgical applications of compliant mechanisms: A review, Journal of mechanisms and robotics 13(2) (2021) 020801.

[11] P.-Z. Li, X.-D. Wang, Y.-X. Sui, D.-F. Zhang, D.-F. Wang, L.-J. Dong, M.-Y. Ni, Piezoelectric actuated phase shifter based on external laser interferometer: Design, control and experimental validation, Sensors 17(4) (2017) 838.

[12] L. Zhao, X. Yu, P. Li, Y. Qiao, High-precision compliant mechanism for lens xy micro-adjustment, Review of Scientific Instruments 91(3) (2020) 035004.

[13] B. Ando, S. Baglio, G. L'Episcopo, C. Trigona, Investigation on mechanically bistable mems devices for energy harvesting from vibrations, Journal of Microelectromechanical Systems 21(4) (2012) 779–790.

[14] H. Shi, H.-J. Su, N. Dagalakis, A stiffness model for control and analysis of a MEMS hexapod nanopositioner, Mechanism and Machine Theory 80 (2014) 246 – 264.

[15] K. Saito, K. Iwata, Y. Ishihara, K. Sugita, M. Takato, F. Uchikoba, Miniaturized rotary actuators using shape memory alloy for insect-type mems microrobot, Micromachines 7(4) (2016) 58.

[16] G. Hao, J. Zhu, Design of a monolithic double-slider based compliant gripper with large displacement and anti-buckling ability, Micromachines 10(10) (2019) 665.

[17] T. J. Teo, G. Yang, I.-M. Chen, A large deflection and high payload flexure-based parallel manipulator for uv nanoimprint lithography: Part i. modeling and analyses, Precision Engineering 38(4) (2014) 861–871.

[18] K. Xu, H. Luo, J. Qin, M. Yang, S. Guo, L. Wang, Flexible devices fabricated by a plate-to-roll nanoimprint lithography system, Nanotechnology 30(7) (2018) 075301.

[19] Z. Wu, Q. Xu, Survey on recent designs of compliant micro-/nano-positioning stages, Actuators 7(1) (2018) 5.

[20] A. Al-Jodah, B. Shirinzadeh, M. Ghafarian, T. K. Das, J. Pinskier, Design, modeling, and control of a large range 3-dof micropositioning stage, Mechanism and Machine Theory 156 (2021) 104159.

[21] T. Wang, Y. Li, Y. Zhang, R. Lin, J. Qian, Z. Dou, Design of a flexure-based parallel xy micropositioning stage with millimeter workspace and high bandwidth, Sensors and Actuators A: Physical (2021) 112899.

[22] P. P. Valentini, M. Cirelli, E. Pennestrì, Second-order approximation pseudo-rigid model of flexure hinge with parabolic variable thickness, Mechanism and Machine Theory 136 (2019) 178–189.

[23] D. F. Machekposhti, N. Tolou, J. L. Herder, A review on compliant joints and rigid-body constant velocity universal joints toward the design of compliant homokinetic couplings, Journal of Mechanical Design 137(3) (2015) 032301.

[24] H. Zhao, C. Zhao, S. Ren, S. Bi, Analysis and evaluation of a near-zero stiffness rotational flexural pivot, Mechanism and Machine Theory 135 (2019) 115–129.

[25] P. Bilancia, G. Berselli, S. Magleby, L. Howell, On the modeling of a contact-aided cross-axis flexural pivot, Mechanism and Machine Theory 143 (2020) 103618.

[26] K. Tolman, E. Merriam, L. Howell, Compliant constant-force linear-motion mechanism, Mechanism and Machine Theory 106 (2016) 68–79.

[27] P. Wang, Q. Xu, Design and modeling of constant-force mechanisms: A survey, Mechanism and Machine Theory 119 (2018) 1–21.

[28] P. Bilancia, G. Berselli, Design and testing of a monolithic compliant constant force mechanism, Smart Materials and Structures 29(4) (2020) 044001.

[29] Y. S. Oh, S. Kota, Synthesis of Multistable Equilibrium Compliant Mechanisms Using Combinations of Bistable Mechanisms, Journal of Mechanical Design 131(2) (2009) 021002.

[30] V. Cavalieri, A. D. Gaspari, S. Ricci, Optimization of compliant adaptive structures in the design of a morphing droop nose, Smart Materials and Structures 29(1) (2020) 075020.

[31] R. J. Lang, K. A. Tolman, E. B. Crampton, S. P. Magleby, L. L. Howell, A review of thickness-accommodation techniques in origami-inspired engineering, Applied Mechanics Reviews 70(1) (2018) 010805.

[32] T. G. Nelson, A. Avila, L. L. Howell, J. L. Herder, D. F. Machekposhti, Origami-inspired sacrificial joints for folding compliant mechanisms, Mechanism and Machine Theory 140 (2019) 194–210.

[33] P. Bilancia, G. Berselli, An overview of procedures and tools for designing nonstandard beam-based compliant mechanisms, Computer-Aided Design 134 (2021) 103001.

[34] M. Ling, L. L. Howell, J. Cao, G. Chen, Kinetostatic and dynamic modeling of flexure-based compliant mechanisms: A survey, Applied Mechanics Reviews 72(3) (2020). 030802.

[35] A. Zhang, G. Chen, A comprehensive elliptic integral solution to the large deflection problems of thin beams in compliant mechanisms, Journal of Mechanisms and Robotics 5(2) (2013) 021006.

[36] L. L. Howell, A. Midha, T. W. Norton, Evaluation of equivalent spring stiffness for use in a pseudo-rigid-body model of large-deflection compliant mechanisms, Journal of Mechanical Design 118(1) (1996) 126–131.

[37] M. Jin, Z. Yang, C. Ynchausti, B. Zhu, X. Zhang, L. L. Howell, Large-deflection analysis of general beams in contact-aided compliant mechanisms using chained pseudo-rigid-body model, Journal of Mechanisms and Robotics 12(3) (2020) 031005.

[38] F. Ma, G. Chen, Modeling large planar deflections of flexible beams in compliant mechanisms using chained beam-constraint-model, Journal of Mechanisms and Robotics 8(2) (2016) 021018.

[39] G. Chen, F. Ma, G. Hao, W. Zhu, Modeling large deflections of initially curved beams in compliant mechanisms using chained beam constraint model, Journal of Mechanisms and Robotics 11(1) (2019) 011002.

[40] G. Hao, J. Yu, H. Li, A brief review on nonlinear modeling methods and applications of compliant mechanisms, Frontiers of Mechanical Engineering 11 (2016) 119–128.

[41] A. Shooshtari, R. Khajavi, An efficient procedure to find shape functions and stiffness matrices of nonprismatic euler–bernoulli and timoshenko beam elements, European Journal of Mechanics - A/Solids 29(5) (2010) 826–836.

[42] G. Balduzzi, M. Aminbaghai, E. Sacco, J. Füssl, J. Eberhardsteiner, F. Auricchio, Non-prismatic beams: A simple and effective timoshenko-like model, International Journal of Solids and Structures 90 (2016) 236–250.

[43] N. Lobontiu, J. S. Paine, E. Garcia, M. Goldfarb, Design of symmetric conic-section flexure hinges based on closed-form compliance equations, Mechanism and machine theory 37(5) (2002) 477–498.

[44] N. Lobontiu, J. S. Paine, E. O'Malley, M. Samuelson, Parabolic and hyperbolic flexure hinges: flexibility, motion precision and stress characterization based on compliance closed-form equations, Precision Engineering 26(2) (2002) 183–192.

[45] N. Lobontiu, J. S. N. Paine, E. Garcia, M. Goldfarb, Corner-filleted flexure hinges, Journal of Mechanical Design 123(3) (2000) 346–352.

[46] Y. Tian, B. Shirinzadeh, D. Zhang, Y. Zhong, Three flexure hinges for compliant mechanism designs based on dimensionless graph analysis, Precision Engineering 34(1) (2010) 92–100.

[47] R. C. Shi, W. Dong, Z. J. Du, Design methodology and performance analysis of application-oriented flexure hinges, Review of Scientific Instruments 84(7) (2013) 075005.

[48] N.-H. Nguyen, M.-Y. Lee, J.-S. Kim, D.-Y. Lee, Compliance matrix of a single-bent leaf flexure for a modal analysis, Shock and Vibration 2015 (2015) 1–10.

[49] R. M. Rivello, Theory and analysis of flight structures, McGraw-Hill, London, 1969.

[50] M. B. Fuchs, The unit-load method, in: Structures and Their Analysis, Springer International Publishing, 2016, pp. 85–110.

[51] Q. Li, C. Pan, X. Xu, Closed-form compliance equations for power-function-shaped flexure hinge based on unit-load method, Precision Engineering 37(1) (2013) 135–145.

[52] G. Chen, X. Shao, X. Huang, A new generalized model for elliptical arc flexure hinges, Review of Scientific Instruments 79(9) (2008) 095103.

[53] G. Chen, X. Liu, H. Gao, J. Jia, A generalized model for conic flexure hinges, Review of Scientific Instruments 80(5) (2009) 055106.

[54] R. R. Vallance, B. Haghighian, E. R. Marsh, A unified geometric model for designing elastic pivots, Precision Engineering 32(4) (2008) 278–288.

[55] W. O. Schotborgh, F. G. Kokkeler, H. Tragter, F. J. van Houten, Dimensionless design graphs for flexure elements and a comparison between three flexure elements, Precision Engineering 29(1) (2005) 41–47.

[56] Q. Meng, Y. Li, J. Xu, New empirical stiffness equations for corner-filleted flexure hinges, Mechanical Sciences 4(2) (2013) 345–356.

[57] T.-M. Li, J.-L. Zhang, Y. Jiang, Derivation of empirical compliance equations for circular flexure hinge considering the effect of stress concentration, International Journal of Precision Engineering and Manufacturing 16 (2015) 1735–1743.

[58] S. T. Smith, V. G. Badami, J. S. Dale, Y. Xu, Elliptical flexure hinges, Review of Scientific Instruments 68(3) (1997) 1474–1483.

[59] H. Wang, X. Zhang, Input coupling analysis and optimal design of a 3-DOF compliant micro-positioning stage, Mechanism and Machine Theory 43(4) (2008) 400–410.

[60] B. K. Donaldson, Analysis of Aircraft Structures, Cambridge University Press, 2008.

[61] P. R. Ouyang, W. J. Zhang, M. M. Gupta, A new compliant mechanical amplifier based on a symmetric five-bar topology, Journal of Mechanical Design 130(10) (2008) 104501.

[62] L. U. Odhner, A. M. Dollar, The smooth curvature model: An efficient representation of euler–bernoulli flexures as robot joints, IEEE Transactions on Robotics 28(4) (2012) 761–772.

[63] Q. Xu, Design and development of a novel compliant gripper with integrated position and grasping/interaction force sensing, IEEE Transactions on Automation Science and Engineering 14(3) (2017) 1415–1428.

[64] X. Sun, B. Yang, A new methodology for developing flexure-hinged displacement amplifiers with micro-vibration suppression for a giant magnetostrictive micro drive system, Sensors and Actuators A: Physical 263 (2017) 30–43.

[65] N. Lobontiu, Compliance-based matrix method for modeling the quasi-static response of planar serial flexure-hinge mechanisms, Precision Engineering 38(3) (2014) 639–650.

[66] W. Chen, X. Zhang, S. Fatikow, Design, modeling and test of a novel compliant orthogonal displacement amplification mechanism for the compact micro-grasping system, Microsystem Technologies 23(7) (2016) 2485–2498.

[67] B. J. Kenton, K. K. Leang, Design and control of a three-axis serial-kinematic high-bandwidth nanopositioner, IEEE/ASME Transactions on Mechatronics 17(2) (2012) 356–369.

[68] M. Ling, J. Cao, L. L. Howell, M. Zeng, Kinetostatic modeling of complex compliant mechanisms with serial-parallel substructures: A semi-analytical matrix displacement method, Mechanism and Machine Theory 125 (2018) 169–184.

[69] W.-L. Zhu, Z. Zhu, P. Guo, B.-F. Ju, A novel hybrid actuation mechanism based XY nanopositioning stage with totally decoupled kinematics, Mechanical Systems and Signal Processing 99 (2018) 747–759.

[70] P. Mottard, Y. St-Amant, Analysis of flexural hinge orientation for amplified piezo-driven actuators, Smart Materials and Structures 18(3) (2009) 035005.

[71] Q. Xu, Y. Li, Analytical modeling, optimization and testing of a compound bridge-type compliant displacement amplifier, Mechanism and Machine Theory 46(2) (2011) 183–200.

[72] P. Liu, P. Yan, A new model analysis approach for bridge-type amplifiers supporting nano-stage design, Mechanism and Machine Theory 99 (2016) 176–188.

[73] L. Yuanqiang, L. Wangyu, Analysis of the displacement of distributed compliant parallel-guiding mechanism considering parasitic rotation and deflection on the guiding plate, Mechanism and Machine Theory 80 (2014) 151–165.

[74] Y. Luo, W. Liu, L. Wu, Analysis of the displacement of lumped compliant parallel-guiding mechanism considering parasitic rotation and deflection on the guiding plate and rigid beams, Mechanism and Machine Theory 91 (2015) 50–68.

[75] Y. Kurita, F. Sugihara, J. Ueda, T. Ogasawara, Piezoelectric tweezer-type end effector with force- and displacement-sensing capability, IEEE/ASME Transactions on Mechatronics 17(6) (2012) 1039–1048.

[76] Y. K. Yong, S. O. R. Mohemani, Design of an inertially counterbalanced z -nanopositioner for high-speed atomic force microscopy, IEEE Transactions on Nanotechnology 12(2) (2013) 137–145.

[77] J. Ueda, T. W. Secord, H. H. Asada, Large effective-strain piezoelectric actuators using nested cellular architecture with exponential strain amplification mechanisms, IEEE/ASME Transactions on Mechatronics 15(5) (2010) 770–782.

[78] J. Schultz, J. Ueda, Two-port network models for compliant rhomboidal strain amplifiers, IEEE Transactions on Robotics 29(1) (2013) 42–54.

[79] Z. Du, R. Shi, W. Dong, A piezo-actuated high-precision flexible parallel pointing mechanism: Conceptual design, development, and experiments, IEEE Transactions on Robotics 30(1) (2014) 131–137.

[80] A. E. Albanesi, M. A. Pucheta, V. D. Fachinotti, A new method to design compliant mechanisms based on the inverse beam finite element model, Mechanism and Machine Theory 65 (2013) 14–28.

[81] R. Friedrich, R. Lammering, M. Rösner, On the modeling of flexure hinge mechanisms with finite beam elements of variable cross section, Precision Engineering 38(4) (2014) 915–920.

[82] Y. Li, J. Huang, H. Tang, A compliant parallel XY micromotion stage with complete kinematic decoupling, IEEE Transactions on Automation Science and Engineering 9(3) (2012) 538–553.

[83] H.-J. Su, H. Shi, J. Yu, A symbolic formulation for analytical compliance analysis and synthesis of flexure mechanisms, Journal of Mechanical Design 134(5) (2012) 51009.

[84] H. Tang, Y. Li, Design, analysis, and test of a novel 2-DOF nanopositioning system driven by dual mode, IEEE Transactions on Robotics 29(1) (2013) 650–662.

[85] H.-H. Pham, I.-M. Chen, Stiffness modeling of flexure parallel mechanism, Precision Engineering 29(4) (2005) 467–478.

[86] S. Xiao, Y. Li, Optimal design, fabrication, and control of an XY micropositioning stage driven by electromagnetic actuators, IEEE Transactions on Industrial Electronics 60(10) (2013) 4613–4626.

[87] J. Qu, W. Chen, J. Zhang, W. Chen, A piezo-driven 2-DOF compliant micropositioning stage with remote center of motion, Sensors and Actuators A: Physical 239 (2016) 114–126.

[88] W. Dong, F. Chen, F. Gao, M. Yang, L. Sun, Z. Du, J. Tang, D. Zhang, Development and analysis of a bridge-lever-type displacement amplifier based on hybrid flexure hinges, Precision Engineering 54 (2018) 171–181.

[89] G. Krishnan, C. Kim, S. Kota, An intrinsic geometric framework for the building block synthesis of single point compliant mechanisms, Journal of Mechanisms and Robotics 3(1) (2010) 011001.

[90] Z. Zhu, S. To, W.-L. Zhu, Y. Li, P. Huang, Optimum design of a piezo-actuated triaxial compliant mechanism for nanocutting, IEEE Transactions on Industrial Electronics 65(8) (2018) 6362–6371.

[91] M. Arredondo-Soto, E. Cuan-Urquizo, A. Gómez-Espinosa, The compliance matrix method for the kinetostatic analysis of flexure-based compliant parallel mechanisms: Conventions and general force–displacement cases, Mechanism and Machine Theory 168 (2022) 104583.

[92] M. Verotti, Analysis of the center of rotation in primitive flexures: Uniform cantilever beams with constant curvature, Mechanism and Machine Theory 97 (2016) 29–50.

[93] M. Verotti, Effect of initial curvature in uniform flexures on position accuracy, Mechanism and Machine Theory 119 (2018) 106–118.

[94] M. Verotti, A pseudo-rigid body model based on finite displacements and strain energy, Mechanism and Machine Theory 149 (2020) 103811.

[95] K. Culmann, Die graphische Statik, Meyer & Zeller, Zurich, 1875.

[96] W. Ritter, Anwendungen der graphischen statik, volume 1, Meyer & Zeller, Zurich, 1888.

[97] D. Capecchi, La scienza delle costruzioni in Italia nell'Ottocento, Springer Milan, 2011.

[98] R. Ferrari, E. Rizzi, On the theory of the ellipse of elasticity as a natural discretisation method in the design of paderno d'adda bridge (italy), in: Structural Analysis of Historic Construction: Preserving Safety and Significance, CRC Press, 2008, pp. 603–612.

[99] M. Faggella, Graphical modal analysis and earthquake statics of linear one-way asymmetric single-story structure, COMPDYN 2013 4th ECCOMAS Thematic Conference on Computational Methods in Structural Dynamics and Earthquake Engineering. Kos Island, Greece (2013).

[100] M. Faggella, R. Gigliotti, C. Morrone, E. Spacone, Mohr circle-based graphical vibration analysis and earthquake response of asymmetric systems, Procedia Engineering 199 (2017) 128–133. X International Conference on Structural Dynamics, EURODYN 2017.

[101] J. Gallier, Basics of Projective Geometry, Springer, New York, 2011, pp. 103–175.

[102] G. Glaeser, H. Stachel, B. Odehnal, The Universe of Conics, Springer Spektrum Berlin, Heidelberg, 2016.

[103] O. Bottema, B. Roth, Theoretical kinematics, volume 24, Courier Dover Publications, New York, 1990.

[104] O. Belluzzi, Scienza delle Costruzioni, vol. II, Zanichelli, Bologna, 1942.

[105] V. Franciosi, Fondamenti di Scienza delle Costruzioni, vol. III Teoria delle Strutture, Liguori, Napoli, 1988.